42p.

VIRGINIA POLYTECHNIC INSTITUTE AND STATE UNIVERSITY

ENGINEERING SCIENCE AND MECHANICS DEPARTMENT

BLACKSBURG, VIRGINIA 24061

IN-31456

A Progress Report on

IDENTIFICATION AND CONTROL OF STRUCTURES IN SPACE

NASA Research Grant NAG-1-225

Covering the Period

July 1 - December 31, 1985

Principal Investigator: Leonard Meirovitch
University Distinguished Professor

Abstract

Work during the period July 1 - December 31, 1985, has concentrated on the application of the equations derived in the preceding period to the maneuvering and vibration suppression of the Spacecraft Control Laboratory Experiment (SCOLE) model. Two different situations have been considered: 1) a space environment and 2) a laboratory environment. This report covers the first case and consists of a paper entitled "Maneuvering and Vibration Control of Flexible Spacecraft", presented at the Workshop on Structural Dynamics and Control Interaction of Flexible Structures, Marshall Space Flight Center, Huntsville, AL, April 22-24, 1986. The second case will be covered in the report for the next period.

MANEUVERING AND VIBRATION CONTROL OF FLEXIBLE SPACECRAFT*

by

L. Meirovitch† & R. D. Quinn†

Virginia Polytechnic Institute & State University

Department of Engineering Science & Mechanics

Blacksburg, Virginia 24061

* Supported by the NASA Research Grant NAG-1-225 sponsored by the Spacecraft Control Branch, Langley Research Center.

† University Distinguished Professor. Fellow AIAA.

†† Graduate Research Assistant. Now Assistant Professor, Department of Mechanical and Aerospace Engineering, Case Western Reserve University, Cleveland, OH, 44106.

ABSTRACT

This paper is concerned with slewing a large structure in space and suppressing any vibration at the same time. The structure is assumed to undergo large rigid-body motions and small elastic deformations. A perturbation method permits a maneuver strategy independent of the vibration control. Optimal control and pole placement techniques, formulated to include actuator dynamics, are used to suppress the vibration during maneuver. The theory is illustrated by simultaneous maneuvering and vibration control of the Spacecraft Control Laboratory Experiment (SCOLE) model in a space environment.

I. INTRODUCTION

The problem of simultaneous maneuver and vibration suppression of spacecraft is becoming increasingly important. Some projected NASA missions involve experiments consisting of the control of flexible bodies carried by a shuttle in an earth orbit. Other missions involve laboratory simulations of similar experiments. The equations of motion for both types of experiments have been presented previously (Ref. 1). A perturbation technique permitting the maneuver strategy to be formulated independently of the vibration problem was also presented. In a following investigation, a straightforward rotational maneuver strategy and an efficient vibration simulation technique were presented (Ref. 2). Rotational maneuvers were shown to cause structural vibrations. The purpose of this paper is to develop ways of suppressing these vibrations during the maneuver by means of feedback control.

Turner and Junkins (Ref. 3), Turner and Chun (Ref. 4) and Breakwell (Ref. 5) addressed the problem of rotational maneuvering and simultaneous vibration suppression of flexible spacecraft for two-

dimensional models. In all cases, the methods used represent extensions of rigid-body maneuvering techniques, requiring the solution of a two point boundary-value problem. The maneuver and vibration control problems are coupled and numerical difficulties arise as the order of the system increases (Ref. 5). Baruh and Silverberg first suggested separating the maneuver and vibration control problems (Ref. 6). However, the vibration control did not include feedback on the rigid-body modes, so that the spacecraft orientation could not be corrected during the open-loop maneuver.

The equations of motion of a flexible spacecraft consist of six nonlinear ordinary differential equations for the rigid-body motion of a reference frame attached to the spacecraft in undeformed state coupled with a set of partial differential equations for the vibration of the elastic members relative to the rigid frame. Hence, the equations describing the motion of a flexible spacecraft during a certain maneuver represent a set of nonlinear hybrid differential equations. In general, hybrid systems of equations do not permit closed-form solution, so that one must consider an approximate solution, which implies spatial discretization and truncation.

The nonlinear equations of motion can be solved by a perturbation approach. The approach consists of separating the equations into a set of equations for the rigid-body motions, representing zero-order effects, and a set of equations for the small elastic motions and deviations from the rigid-body motions, representing first-order effects. The perturbation technique permits a maneuver strategy that is independent of the elastic vibration.

The order of the perturbation equations for the vibration suppression is often so large that some reduction is necessary. To this end, the elastic motion can be expanded into a series consisting of premaneuver eigenvectors acting as admissible vectors. These admissible vectors clearly do not decouple the equations of motion, but using a smaller number than the order of the system permits a reduction in the order. We refer to the corresponding equations as quasi-modal equations. The task of simulation and vibration control can be carried out conveniently by means of the quasi-modal equations.

At each sampling time, the control forces are formulated as if the premaneuver eigenfunctions are the true eigenfuctions at that time. This results in a modeling error, but this error does not create a stability problem for robust control techniques, such as natural control, which do not require the exact eigenfunctions in control formulation (Refs. 7-11).

Any maneuver can be regarded as a single-axis rotation, where in general the axis of rotation is not a principal axis. The single-axis maneuver has the advantage of simplifying the matrices of time-dependent coefficients in the perturbation equations. The rigid-body maneuver represents an open-loop control strategy for minimum-time, single-axis rotation about an axis which is not necessarily a principal axis.

The vibration control is carried out in discrete time, which amounts to regarding the system as having constant coefficient over the duration of any sampling period. This permits the use of control algorithms developed for time-invariant systems, such as optimal control and pole placement. Actuator dynamics can degrade the performace of the control system. The inclusion of actuator dynamics requires a

reformulation of the vibration control techniques mentioned above. The theory is illustrated by simultaneous maneuvering and vibration control of the SCOLE model in a space environment.

II. EQUATIONS OF MOTION

We consider a space system consisting of a shuttle carrying an antenna connected to the shuttle by means of a mast, as shown in Fig. 1. The shuttle is assumed to be rigid and the mast and antenna are deformable. The motion of the spacecraft is referred to a given reference frame $x_0y_0z_0$ embedded in the rigid shuttle (Fig. 1). The reference frame has six degrees of freedom, three rigid-body rotations and three rigid-body translations. We propose to derive the equations of motion by means of the Lagrangian approach, which requires the expressions for the kinetic energy, potential energy and virtual work. Considering Fig. 1, the position of a point S in the rigid shuttle relative to the inertial frame XYZ is $\underset{\sim}{R}_S = \underset{\sim}{R} + \underset{\sim}{r}$. Moreover, the position of a point A on the elastic appendage is $\underset{\sim}{R}_A = \underset{\sim}{R} + \underset{\sim}{a} + \underset{\sim}{u}$, where $\underset{\sim}{u}$ is the elastic displacement. The velocities of these points are then

$$\dot{\underset{\sim}{R}}_S = \dot{\underset{\sim}{R}} + \underset{\sim}{\omega} \times \underset{\sim}{r} \tag{1}$$

$$\dot{\underset{\sim}{R}}_A = \dot{\underset{\sim}{R}} + \underset{\sim}{\omega} \times (\underset{\sim}{a} + \underset{\sim}{u}) + \dot{\underset{\sim}{u}} \tag{2}$$

where $\dot{\underset{\sim}{R}}$ and $\underset{\sim}{\omega}$ are the translational and angular velocities of the frame $x_0y_0z_0$ with respect to the inertial frame, respectively, and $\dot{\underset{\sim}{u}}$ is the elastic velocity of the point relative to $x_0y_0z_0$. Hence, the kinetic energy of the spacecraft is

$$T = \frac{1}{2}\int_{m_S} |\dot{\underset{\sim}{R}}_S|^2 dm_S + \frac{1}{2}\int_{m_A} |\dot{\underset{\sim}{R}}_A|^2 dm_A \tag{3}$$

where m_S and m_A are the masses of the shuttle and appendage, respectively.

The potential energy is due to the combined effects of gravity and strain energy. The gravitational potential can be expresssed as

$$V_g = - Gm_e[\int_{m_S} |\underset{\sim}{R} + \underset{\sim}{r}|^{-1} dm_S + \int_{m_A} |\underset{\sim}{R} + \underset{\sim}{a} + \underset{\sim}{u}|^{-1} dm_A] \tag{4}$$

where m_e is the mass of the earth and G is the universal gravitational constant. The strain energy can be expressed as an energy inner product denoted by [,] (Ref. 12). This includes centrifugal and gravitational stiffening effects on the appendage. The total potential energy then becomes

$$V = \frac{1}{2}[\underset{\sim}{u},\underset{\sim}{u}] + V_g \tag{5}$$

Denoting by $\underset{\sim}{f}_S$ and $\underset{\sim}{f}_A$ the force vectors per unit volume of the shuttle and appendage, respectively, we can express the virtual work as

$$\delta W = \int_{D_S} \underset{\sim}{f}_S \cdot \delta \underset{\sim}{R}_S \, dD_S + \int_{D_A} \underset{\sim}{f}_A \cdot \delta \underset{\sim}{R}_A \, dD_A \tag{6}$$

where D_S and D_A are the domains of the shuttle and appendage, respectively. The system is discretized in space by expressing the elastic displacements vector in the form

$$\underset{\sim}{u} = \Phi \underset{\sim}{q} \tag{7}$$

where Φ is a matrix of space-dependent admissible functions and $\underset{\sim}{q}$ is a vector of time-dependent generalized coordinates. The kinetic and potential energies and virtual work can be expressed in matrix form by introducing a rotational transformation matrix C from the XYZ frame to the $x_0y_0z_0$ frame, where the elements of C are nonlinear functions of a set of Euler angles α_1, α_2, α_3. Lagrange's equations of motion can then be written in the symbolic form

$$\frac{d}{dt}\left(\frac{\partial T}{\partial \dot{\underset{\sim}{R}}}\right) + \frac{\partial V}{\partial \underset{\sim}{R}} = C^T \underset{\sim}{F} \tag{8a}$$

$$\frac{d}{dt}\left(\frac{\partial T}{\partial \dot{\underset{\sim}{\alpha}}}\right) - \frac{\partial T}{\partial \underset{\sim}{\alpha}} + \frac{\partial V}{\partial \underset{\sim}{\alpha}} = D^T \underset{\sim}{M} \tag{8b}$$

$$\frac{d}{dt}\left(\frac{\partial T}{\partial \dot{\underset{\sim}{q}}}\right) - \frac{\partial T}{\partial \underset{\sim}{q}} + \frac{\partial V}{\partial \underset{\sim}{q}} = \underset{\sim}{Q} \tag{8c}$$

where the matrix D is defined by the expression

$$\underset{\sim}{\omega} = D(\underset{\sim}{\alpha})\dot{\underset{\sim}{\alpha}} \tag{9}$$

The resulting equations of motion are nonlinear due to the large rigid-body motion.

III. PERTURBATION METHOD

Consider a first-order perturbation on the quantities $\underset{\sim}{R}$ and $\underset{\sim}{\alpha}$

$$\underset{\sim}{R} = \underset{\sim}{R}_0 + \underset{\sim}{R}_1 \ , \quad \underset{\sim}{\alpha} = \underset{\sim}{\alpha}_0 + \underset{\sim}{\alpha}_1 \tag{10a,b}$$

where the first-order terms $\underset{\sim}{R}_1$ and $\underset{\sim}{\alpha}_1$ are small compared to the zero-order terms $\underset{\sim}{R}_0$ and $\underset{\sim}{\alpha}_0$. Introducing Eqs. (10) into the nonlinear equations of motion and separating orders of magnitude, we obtain zero-order and first-order perturbation equations. Before proceeding with this technique, we first develop some expressions relating the perturbations α_{11}, α_{21}, α_{31} in the Euler angles, α_1, α_2, α_3 with small angular deflections β_1, β_2, β_3 expressed in the body-fixed frame. This will permit expressing all the variables in the perturbation equations in terms of components along the $x_0y_0z_0$ axes.

It can be shown that the vector of body-fixed perturbation angles can be related to the vector of perturbed Euler angles by

$$\underset{\sim}{\beta} = D(\underset{\sim}{\alpha}_0)\underset{\sim}{\alpha}_1 \tag{11}$$

The perturbed angular velocity vector can then be expressed as

$$\underset{\sim}{\omega} \cong \underset{\sim}{\omega}_0 + \underset{\sim}{\omega}_1 \ , \quad \underset{\sim}{\omega}_1 = \tilde{\underset{\sim}{\omega}}_0^T\underset{\sim}{\beta} + \dot{\underset{\sim}{\beta}} \tag{12,13}$$

In keeping with our objective of expressing the first-order perturbation equations in the body-fixed frame, Eq. (10a) is replaced by

$$\underset{\sim}{R} = \underset{\sim}{R}_0 + C_0^T\underset{\sim}{R}_1 \tag{14}$$

where $\underset{\sim}{R}_1$ is now a vector measured with respect to axes $x_0y_0z_0$ and the

rotation matrix has the perturbed form

$$C \cong C_0 + C_1 \ , \ C_1 = \tilde{\beta} C_0 \tag{15a,b}$$

The applied forces and moments can also be expressed in first-order perturbed form as follows:

$$\underset{\sim}{F} = \underset{\sim}{F}_0 + \underset{\sim}{F}_1 \ , \quad \underset{\sim}{M} = \underset{\sim}{M}_0 + \underset{\sim}{M}_1 \tag{16a,b}$$

The zero-order equations of motion, which govern the structure as if it were rigid, can be expressed as

$$m\ddot{\underset{\sim}{R}}_0 + C_0^T \tilde{\underset{\sim}{S}}_0 \dot{\underset{\sim}{\omega}}_0 + C_0^T \tilde{\underset{\sim}{\omega}}_0^T \tilde{\underset{\sim}{S}}_0 \underset{\sim}{\omega}_0 + \frac{Gm_e}{|\underset{\sim}{R}_0|^3} \left[m\underset{\sim}{R}_0 + (I - 3\hat{\underset{\sim}{R}}_0 \hat{\underset{\sim}{R}}_0^T) C_0^T \underset{\sim}{S}_0 \right] = C_0^T \underset{\sim}{F}_0 \tag{17a}$$

$$\tilde{\underset{\sim}{S}}_0^T C_0 \ddot{\underset{\sim}{R}}_0 + \frac{Gm_e}{|\underset{\sim}{R}_0|^3} \tilde{\underset{\sim}{S}}_0^T C_0 \underset{\sim}{R}_0 + I_0 \dot{\underset{\sim}{\omega}}_0 + \tilde{\underset{\sim}{\omega}}_0^T I_0 \underset{\sim}{\omega}_0 = \underset{\sim}{M}_0 \tag{17b}$$

where $\hat{\underset{\sim}{R}}_0$ is a unit vector in the direction of $\underset{\sim}{R}_0$, I_0 is the mass moment of inertia matrix about point O, m is the mass of the spacecraft and

$$\underset{\sim}{S}_0 = \int_{m_S} \underset{\sim}{r} \, dm_S + \int_{m_A} \underset{\sim}{a} \, dm_A \tag{18}$$

The first-order linear perturbation equations, which govern the vibrational motion of the structure, can be expressed in the matrix form

$$M\ddot{\underset{\sim}{x}} + G\dot{\underset{\sim}{x}} + (K_S + K_{NS})\underset{\sim}{x} = \underset{\sim}{F}^* \tag{19}$$

where

$$\underset{\sim}{x}^T = [\underset{\sim}{R}_1^T \ \ \underset{\sim}{\beta}^T \ \ \underset{\sim}{q}^T] \ , \ \underset{\sim}{F}^{*T} = [\underset{\sim}{F}_1^T \ \ \underset{\sim}{M}_1^T \ \ \underset{\sim}{Q}_0^T + \underset{\sim}{Q}_1^T] \tag{20a,b}$$

$$M = \begin{bmatrix} M_0 & \tilde{\underset{\sim}{S}}_0 & \bar{\Phi} \\ \tilde{\underset{\sim}{S}}_0^T & I_0 & \tilde{\Phi} \\ \bar{\Phi}^T & \tilde{\Phi}^T & M_A \end{bmatrix} \quad M_0 = \begin{bmatrix} m & 0 & 0 \\ 0 & m & 0 \\ 0 & 0 & m \end{bmatrix} \tag{20c,d}$$

$$G = \begin{bmatrix} 2M_0\tilde{\omega}_0^T & 2\tilde{\omega}_0^T\tilde{S}_0 & 2\tilde{\omega}_0^T\bar{\Phi} \\ -2(\tilde{\omega}_0^T\tilde{S}_0)^T & I_0\tilde{\omega}_0^T + \tilde{\omega}_0^T I_0 + [\widetilde{I_0\omega_0}] & \tilde{\omega}_0^T\tilde{\Phi} + J_0 \\ -2(\tilde{\omega}_0^T\bar{\Phi})^T & -[\tilde{\omega}_0^T\tilde{\Phi} + J_0]^T & 2\tilde{L}_A \end{bmatrix} \tag{20e}$$

$$K_S = \begin{bmatrix} M_0[\tilde{\omega}_0^2 + \bar{H}] & \tilde{F}_0^T + [\tilde{\omega}_0^2 + \bar{H}]\tilde{S}_0 & [\tilde{\omega}_0^2 + \bar{H}]\bar{\Phi} \\ \tilde{F}_0 + \tilde{S}_0^T[\tilde{\omega}_0^2 + \bar{H}] & \tilde{\omega}_0 I_0\tilde{\omega}_0 & \tilde{\omega}_0^T J_0 + \tilde{H}\bar{\Phi} \\ \bar{\Phi}^T[\tilde{\omega}_0^2 + \bar{H}] & J_0^T\tilde{\omega}_0 + \bar{\Phi}^T\tilde{H}^T & \bar{L}_A + K_A \end{bmatrix} \tag{20f}$$

$$K_{NS} = \begin{bmatrix} M_0\dot{\tilde{\omega}}_0^T & \dot{\tilde{\omega}}_0^T\tilde{S}_0 & \dot{\tilde{\omega}}_0^T\bar{\Phi} \\ -(\dot{\tilde{\omega}}_0^T\tilde{S}_0)^T & I_0\dot{\tilde{\omega}}_0^T + [\widetilde{I_0\omega_0}]\tilde{\omega}_0^T + \tilde{S}_0\tilde{H} & \dot{J}_0 \\ -(\dot{\tilde{\omega}}_0^T\bar{\Phi})^T & \tilde{\Phi}^T\dot{\tilde{\omega}}_0^T & \dot{\tilde{L}}_A \end{bmatrix} \tag{20g}$$

and

$$\bar{\Phi} = \int_{m_A} \Phi \, dm_A, \quad \tilde{\Phi}^T = \int_{m_A} \Phi^T\tilde{a} \, dm_A \tag{21a,b}$$

$$\tilde{L}_A(\underset{\sim}{\omega}) = \int_{m_A} \Phi^T\tilde{\omega}^T\Phi \, dm_A, \quad \bar{L}_A(\underset{\sim}{\omega}) = \int_{m_A} \Phi^T\tilde{\omega}^2\Phi \, dm_A \tag{21c,d}$$

$$M_A = \int_{m_A} \Phi^T\Phi \, dm_A \quad , \quad J(\underset{\sim}{\omega}) = \int_{m_A} (\tilde{a}\tilde{\omega} + [\tilde{a}\underset{\sim}{\omega}])\Phi \, dm_A \tag{21e,f}$$

IV. RIGID-BODY MANEUVER

The perturbation method permits the maneuver strategy to be designed independently of the vibration control. Indeed, a straightforward single-axis minimum-time maneuver strategy is developed in Ref. 2. It is shown in Ref. 2 that the axis of rotation need not be a principal axis, so that any general rotational maneuver is possible. The maneuver policy is formulated in continuous time but implemented in discrete time, so that some error can occur. Also, the equations

governing the maneuver are nonlinear, so that the solution of Ref. 2 can be unstable. However, the vibration control includes feedback control of the rigid-body modes and can stabilize the spacecraft as well as reduce the error caused by discrete-time sampling.

The most desirable control technique for a maneuver excites only the desired rigid-body motion, not the elastic modes. From Ref. 2, the components of the maneuver force distribution exhibiting these characteristics can be expressed as

$$F_1(p,t) = x(p)m(p)\dot{\theta}^2(t) \tag{22a}$$

$$F_2(p,t) = -z(p)m(p)\ddot{\theta}(t) \tag{22b}$$

$$F_3(p,t) = y(p)m(p)\ddot{\theta}(t) \tag{22c}$$

where $\theta(t)$ is the desired angular motion, $m(p)$ is the mass density at point p, and $x(p)$, $y(p)$ and $z(p)$ are the components of the position vector of point p with respect to the center of rotation. The actuating forces are proportional to rotational rigid-body modes, so that they will not excite the elastic modes and cause undesirable vibration. Of course, distributed forces can only be implemented approximately with discrete actuators, which tends to excite some vibration. Also, centrifugal forces can cause vibration during the maneuver, so that vibration control may be necessary.

V. QUASI-MODAL EQUATIONS OF MOTION

During the maneuver, the gyroscopic and stiffness matrices, and hence the eigenvalue problem, are functions of time. In Ref. 2, a truncated set of the premaneuver eigenvectors is used as a set of admissible vectors to simplify and reduce the order of the equations of motion to a form called the quasi-modal equations of motion. Using this approach, Eq. (19) can be reduced to the quasi-modal form

$$\ddot{\underset{\sim}{u}}(t) + \bar{G}(t)\dot{\underset{\sim}{u}}(t) + [\Lambda + \bar{K}(t)]\underset{\sim}{u}(t) = \underset{\sim}{f}(t) \tag{23}$$

where

$$\bar{G}(t) = X^T G(t) X, \quad \bar{K}(t) = X^T K_t(t) X \tag{24a,b}$$

are reduced-order gyroscopic and stiffness matrices, $\underset{\sim}{u}$ is a vector of the quasi-modal coordinates defined by

$$\underset{\sim}{x}(t) = X\underset{\sim}{u}(t) \tag{24c}$$

where X is a rectangular matrix of the lower premaneuver eigenvectors normalized so that

$$X^T M X = I \ , \ X^T K_0 X = \Lambda \tag{24d,e}$$

in which K_0 contains the constant terms in the stiffness matrix and Λ is a diagonal matrix of the premaneuver eigenvalues, and

$$\underset{\sim}{f}(t) = X^T \underset{\sim}{F}^*(t) \tag{24f}$$

is the vector of modal forces. Comparing Eq. (23) with Eq. (19), we see that the premaneuver eigenvectors have not decoupled the equations of motion. However, as the maneuver velocity decreases, the time-varying terms decrease in magnitude and the equations approach an uncoupled form. Also note that the mass matrix has been reduced to the identity matrix, which is convenient for casting Eq. (23) in state space form.

VI. VIBRATION CONTROL

The tangential and centrifugal disturbance forces during the maneuver can cause vibration to be suppressed by means of feedback control, as demonstrated in Ref. 2. The perturbation method permits the vibration control to be formulated separately from the maneuver control, resulting in the quasi-modal equations of motion.

a) Actuator Dynamics

The equation of motion for the rth mode can be expressed as

$$\ddot{u}_r(t) + \omega_r^2 u_r(t) = f_{dr}(t) + f_r(t) \tag{25}$$

where $f_{dr}(t)$ is the sum of the rth modal disturbance and maneuver control forces and $f_r(t)$ is the rth modal vibrational control force defined as the rth component of the vector

$$\underset{\sim}{f}(t) = X^T \underset{\sim}{F}(t) \tag{26}$$

where $\underset{\sim}{F}(t)$ is a vector of control forces and moments. The modal disturbance force $f_{dr}(t)$ includes terms arising from $\bar{G}(t)$ and $\bar{K}(t)$, as can be concluded from Eq. (23). These terms are negligible when the maneuver angular velocity is small relative to the lowest natural frequency of vibration and the maneuver angular acceleration is similarly small. The equation governing the output of a typical set of actuators is assumed to have the vector form

$$\dot{\underset{\sim}{F}}(t) = a\underset{\sim}{F}(t) + b\underset{\sim}{F}_c(t) \tag{27}$$

where a and b are constants and $\underset{\sim}{F}_c(t)$ is the command force vector. Multiplying Eq. (27) by X^T, the equation for the rth modal control force can be expressed as

$$\dot{f}_r(t) = af_r(t) + bf_{cr}(t) \tag{28}$$

where f_r and f_{cr} are the rth components of the vectors

$$\underset{\sim}{f} = X^T \underset{\sim}{F} \tag{29a}$$

and

$$\underset{\sim}{f}_c = X^T \underset{\sim}{F}_c \tag{29b}$$

respectively. In discrete time, if the feedback force f_r is computed at t_i, the earliest it can be applied is the next sampling time t_{i+1}. However, considering Eq. (28) in discrete time, f_{cr} is the quantity that is updated at t_{i+1} and the desired force f_r cannot actually be applied until t_{i+2}. This problem can be circumvented by including the actuator dynamics, Eq. (27), in the control formulation.

Using Eq. (25) and assuming that $f_{dr}(t)$ can be neglected, we can write

$$\ddot{u}_r + \omega_r^2 \dot{u}_r = \dot{f}_r \tag{30}$$

Then, introducing Eqs. (25) and (28) into Eq. (30), the combined dynamic equation can be expressed as

$$\dddot{u}_r = -\omega_r^2 \dot{u}_r + a\ddot{u}_r + a\omega_r^2 u_r + bf_{cr} \tag{31}$$

Equation (31) can be rewritten in the state form

$$\dot{\underset{\sim}{z}}_r = A_r \underset{\sim}{z}_r + \underset{\sim}{b} f_{cr} \tag{32}$$

where

$$\underset{\sim}{z}_r^T = [u_r \quad \dot{u}_r \quad \ddot{u}_r] \ , \ \underset{\sim}{b}^T = [0 \quad 0 \quad b] \tag{33a,b}$$

$$A_r = \begin{bmatrix} 0 & 1 & 0 \\ 0 & 0 & 1 \\ a\omega_r^2 & -\omega_r^2 & a \end{bmatrix} \tag{33c}$$

b) Optimal Control

The minimum-time optimal control policy is bang-bang and involves determining three-dimensional switching surfaces for each mode. At each sampling time the modal state is to be located with respect to the switching surfaces, and based on this the command modal force is set at the positive or negative maximum value. The calculation of three-dimensional switching surfaces is not a simple matter and using them in the above mentioned fashion can be computationally time consuming (Ref. 13). If the measured modal states are noisy, the modal forces could be switched frequently. This implies frequent, abrupt structural accelerations which, when applied with spatially-discrete forces, tend to destabilize the uncontrolled modes.

As an alternative, we consider a quadratic performance measure in conjunction with the independent modal-space control (IMSC) method. In particular, we consider a performance index consisting of a weighted sum of the elastic energy and the control effort (Refs. 8, 9). This performance index has the form

$$J = \sum_{r=1}^{\infty} J_r \tag{34}$$

where

$$J_r = \int_0^{\infty} (\underset{\sim}{z}_r^T Q_r \underset{\sim}{z}_r + R_r f_{cr}^2)dt \tag{35}$$

are modal performance indices, in which

$$Q_r = \begin{bmatrix} q_r & 0 & 0 \\ 0 & 1 & 0 \\ 0 & 0 & 0 \end{bmatrix} \tag{36}$$

is a weighting matrix and R_r is a weighting factor. For the elastic modes, q_r is taken as the rth eigenvalue ω_r^2, and for the rigid-body modes q_r is chosen on the basis of pole-placement considerations. As the weight R_r is decreased, the rate of modal energy dissipation is increased and, of course, more effort is required. Hence, R_r can be chosen on the basis of the available control command force for vibration suppression. The command forces required by this performance index tend to be smooth functions. Smooth forcing time histories are preferable in that they do not tend to excite the uncontrolled modes to the extent that forces containing discontinuities do.

To minimize J, each modal performance index J_r can be minimized independently. The steady-state Riccati equation for the rth mode is an algebraic matrix equation of order three and can be expressed as

$$0 = -K_r A_r - A_r^T K_r - Q_r + \frac{1}{R_r} K_r \underset{\sim\sim}{b} \underset{\sim}{b}^T K_r \tag{37}$$

where K_r is a symmetric matrix to be determined; the matrix has the form

$$K_r = \begin{bmatrix} k_{r1} & & \text{symm.} \\ k_{r2} & k_{r4} & \\ k_{r3} & k_{r5} & k_{r6} \end{bmatrix} \tag{38}$$

The linear, state feedback control law is of the form

$$f_{cr} = -\frac{1}{R_r}\,\underset{\sim}{b}^T K_r \underset{\sim}{z}_r \tag{39}$$

Introducing Eqs. (33a,b) into Eq. (39), the control law becomes

$$f_{cr} = -\frac{b}{R_r}\left(k_{r3}u_r + k_{r5}\dot{u}_r + k_{r6}\ddot{u}_r\right) \tag{40}$$

which minimizes the performance index given by Eq. (35) (Ref. 13). In solving Eq. (37), the required entries of K_r can be shown to satisfy the following expressions:

$$k_{r3} = \frac{R_r}{b^2}\left(a\omega_r^2 + d_r\right) \tag{41a}$$

$$k_{r6}^4 C_4 + k_{r6}^3 C_3 + k_{r6}^2 C_2 + k_{r6} C_1 + C_0 = 0 \tag{41b}$$

$$k_{r5} = -ak_{r6} + \frac{b^2}{2R_r}\,k_{r6}^2 \tag{41c}$$

where

$$d_r = \left[a^2\omega_r^4 + q_r b^2/R_r\right]^{1/2},\quad C_0 = \frac{1}{d_r}\left(ak_{r3} - \frac{1}{2}\right) \tag{42a,b}$$

$$C_1 = -\frac{1}{d_r}\left(d_r + a\omega_r^2\right),\quad C_2 = \frac{b^2}{2d_r R_r}\left(\omega_r^2 + a^2\right) \tag{42c,d}$$

$$C_3 = \frac{-b^4 a}{2d_r R_r^2},\quad C_4 = \frac{b^6}{8d_r R_r^3} \tag{42e,f}$$

are constant coefficients which can be evaluated for each mode off-line. The control law given by Eq. (40) is IMSC modified to include actuator dynamics. IMSC is also called natural control because the closed-loop modes are identical to the open-loop or natural modes, so that natural coordinates remain natural after control (Ref. 9). Natural control is efficient because it wastes no effort in changing the shape

of the modes (Ref. 14), as other control techniques do. In this regard, we recall that only eigenvalues affect stability and not eigenvectors.

Equation (40) can be expressed in the form

$$f_{cr} = -g_{r1}u_r - g_{r2}\dot{u}_r - g_{r3}\ddot{u}_r \tag{43}$$

where the control gains are defined as follows:

$$g_{r1} = \frac{bk_{r3}}{R_r} \quad , \quad g_{r2} = \frac{bk_{r5}}{R_r} \quad , \quad g_{r3} = \frac{bk_{r6}}{R_r} \tag{44a-c}$$

Introducing Eq. (43) into Eq. (32), considering Eqs. (33) and expanding the characteristic determinant, we conclude that the closed-loop poles must satisfy the equation

$$s^3 + (bg_{r3} - a)s^2 + (bg_{r2} + \omega_r^2)s + (bg_{r1} - a\omega_r^2) = 0 \tag{45}$$

c) Pole Allocation

In optimal control, a performance measure is defined, perhaps arbitrarily, and minimized. The pole-allocation method is a modal control method in which the poles are chosen for each mode, again somewhat arbitrarily, and the actuator forces are computed to produce these preselected poles. The most general form of the poles for the rth mode defined by Eqs. (32) and (33), and whose characteristic equation is represented by Eq. (45), can be expressed as

$$s_{r1} = \alpha_r + i\beta_r, \; s_{r2} = \alpha_r - i\beta_r, \; s_{r3} = \gamma_r \tag{46a-c}$$

where α_r and γ_r are related to the time constants for the rth mode and β_r is the closed-loop modal frequency. The characteristic equation associated with the poles given by Eqs. (46) is

$$s^3 + (-\gamma_r - 2\alpha_r)s^2 + (2\gamma_r\alpha_r + \alpha_r^2 + \beta_r^2)s + (-\gamma_r\alpha_r^2 - \gamma_r\beta_r^2) = 0 \tag{47}$$

Comparing Eqs. (47) and (45), we obtain the control gains

$$g_{r1} = \frac{1}{b}\left[a\omega_r^2 - \gamma_r(\alpha_r^2 + \beta_r^2)\right] \tag{48a}$$

$$g_{r2} = \frac{1}{b}(2\gamma_r\alpha_r + \alpha_r^2 + \beta_r^2 - \omega_r^2), \; g_{r3} = \frac{1}{b}(a - 2\alpha_r - \gamma_r) \tag{48b,c}$$

Hence, the poles given by Eqs. (46) can be chosen for each mode and implemented with the command modal force given by Eq. (43) and the gains of Eqs. (48).

d) Implementation of Modal Control

i. Modal actuation

Implementation of any IMSC technique requires an inversion of Eq. (29b), so that the applied command force $\underset{\sim}{F}_C$ can be found from knowledge of the modal command force $\underset{\sim}{f}_C$. For discrete actuators, the simplest implementation technique is a projection method (Ref. 9). Premultiplying Eq. (24d) by the pseudo-inverse of X^T, denoted by X^{-T}, we obtain

$$X^{-T} = MX \tag{49}$$

Premultiplying Eq. (29b) by X^{-T} and considering Eq. (49), we obtain

$$\underset{\sim}{F}_C = MX\underset{\sim}{f}_C \tag{50}$$

which is the discrete counterpart of a distributed generalized force and must be applied with actuators at every finite element node. This may require an impractically large number of actuators, so that only an approximate "distributed" force can be applied. In the projection technique, distributed control is implemented approximately by means of discrete actuators (Ref. 9).

Another method of calculating the applied command force $\underset{\sim}{F}_C$ requires a numerical inversion (Ref. 8). The advantage of this technique is that it produces a subset of the desired components of the modal force vector exactly, rather than only approximately as in the case of projected control. Hence, this type of control is a true natural control in that the closed-loop eigenfunctions of the controlled modes are identical to the open-loop eigenfunctions. Note that the inversion must be recalculated in the event of an actuator failure. The forces computed

from both the inverse and projected methods tend to excite the uncontrolled modes giving rise to so-called control spillover (Ref. 8, 9).

ii. Modal estimation

Modal state estimation is another common problem inherent in the implementation of modal control techniques. This problem is somewhat analogous to that of modal force implementation. It requires the estimation of $\underset{\sim}{u}(t)$ from measurement of $\underset{\sim}{x}(t)$, which requires premultiplication of Eq. (24c) by the matrix product $X^T M$, so that

$$\underset{\sim}{u}(t) = X^T M \underset{\sim}{x}(t) \tag{51}$$

which is the second half of the expansion theorem (Ref. 12). Equation (51) and its time derivatives form what are known as modal filters (Ref. 15). Application of modal filters presupposes either "distributed" sensors or sensors at every node for a finite element model. An acceptable approach to modal state estimation is to interpolate the discrete sensor measurements by means of admissible functions to produce approximate displacement and velocity profiles, where the latter are functions of the spatial variables. These functions are then introduced into the modal filter equations to yield the approximate modal states.

An alternative approach to modal state estimation involves a numerical inversion of a matrix. In a manner analogous to the inversion technique for force implementation, the displacement vector and modal matrix of Eq. (24c) can be partitioned as follows:

$$\begin{bmatrix} \underset{\sim}{x}_s \\ --- \\ \underset{\sim}{x}_{ns} \end{bmatrix} = \begin{bmatrix} B_s \\ --- \\ B_{ns} \end{bmatrix} \underset{\sim}{u} \tag{52}$$

where $\underset{\sim}{x}_s$ is an s × 1 vector of measured displacements, $\underset{\sim}{x}_{ns}$ is the complement of $\underset{\sim}{x}_s$, B_s is an s × c submatrix of the modal matrix X and B_{ns} is the complement of B_s. Hence, the equation

$$\underset{\sim}{x}_s = B_s \underset{\sim}{u} \tag{53}$$

relates the modal displacements with the measured displacements. Premultiplying Eq. (52) by B_s^{-1}, we obtain

$$\underset{\sim}{u} = B_s^{-1} \underset{\sim}{x}_s \tag{54}$$

where B_s^{-1} is only a pseudo-inverse of B_s if s ≠ c. The expression

$$\underset{\sim}{x}_{ns} = B_{ns} B_s^{-1} \underset{\sim}{x}_s \tag{55}$$

can be regarded as observation spillover. Equation (55) implies assignment of values to the unmeasured components of the displacement vector.

e) Output Feedback Control

Modal control techniques have become quite common in the field of control of structures because of their ability to take advantage of the physical and mathematical properties of the natural modes of vibration. The main drawback common to all modal control methods is the problem encountered in modal state estimation with discrete sensors. Direct feedback, where the command control force is related directly to the measured state through control gains, avoids modal estimation entirely. In addition, if this feedback force is the physical (rather than modal) force, then the modal force implementation is also avoided. Hence, a useful control technique might take advantage of the concepts of natural modes but be applicable to output feedback. To this end, the relationship between linear, output feedback control and linear modal feedback control will now be explored.

Consider a linear control law having the special form

$$\underset{\sim}{F}_c(t) = -A[\underset{\sim}{x}(t)g_1 + \dot{\underset{\sim}{x}}(t)g_2 + \ddot{\underset{\sim}{x}}(t)g_3] \tag{56}$$

where g_1, g_2 and g_3 are control gain factors, $\underset{\sim}{F}_c$ is a vector of actual command forces, $\underset{\sim}{x}$, $\dot{\underset{\sim}{x}}$ and $\ddot{\underset{\sim}{x}}$ vectors of measured displacements, velocities and accelerations and A is a weighting matrix of constant coefficierts. Using Eq. (24c) we obtain

$$\underset{\sim}{F}_c(t) = -AX[\underset{\sim}{u}(t)g_1 + \dot{\underset{\sim}{u}}(t)g_2 + \ddot{\underset{\sim}{u}}(t)g_3] \tag{57}$$

From Eq. (43), however, we conclude that, if the modal control gains are the same for all the modes, then the modal control force can be expressed in the vector form

$$\underset{\sim}{f}_c(t) = -\underset{\sim}{u}(t)g_1 - \dot{\underset{\sim}{u}}(t)g_2 - \ddot{\underset{\sim}{u}}(t)g_3 \tag{58}$$

Hence, Eq. (57) takes the form

$$\underset{\sim}{F}_c = AX\underset{\sim}{f}_c \tag{59}$$

Recalling that Eq. (50) also relates $\underset{\sim}{f}_c$ and $\underset{\sim}{F}_c$, and Eq. (50) is true regardless of the control technique used as it is an integral part of the expansion theorem, it is obvious that the weighting matrix A should be set equal to the mass matrix. Hence, if A is replaced by M in Eq. (56), the output feedback control law takes the form

$$\underset{\sim}{F}_c(t) = -M[\underset{\sim}{x}(t)g_1 + \dot{\underset{\sim}{x}}(t)g_2 + \ddot{\underset{\sim}{x}}g_3] \tag{60}$$

so that the control specified by Eq. (60) is equivalent to the modal control of Eq. (58). However, the control gain factors remain to be determined.

A method of determining a particular set of control gains having good physical and mathematical basis is known as uniform damping control (Ref. 16). To this end, we consider Eqs. (46), which represent the desired closed-loop poles for pole allocation. But, changing the natural frequencies can be regarded as a waste of effort in the case of

vibration suppression. In view of this, we choose s_r in Eqs. (46) as being equal to the natural frequency ω_r of the rth mode. The expansion theorem states that the motion of the structure can be represented as a linear combination of all the modes. Hence, it is reasonable to force all the modes to decay at the same rate of time, which implies that $\alpha_r = \alpha$ and $\gamma_r = \gamma$ in Eqs. (46). Introducing these values into Eqs. (48), the gains for the rth mode can be expressed as

$$g_{r1} = \frac{1}{b}\left[(a - \gamma)\omega_r^2 - \gamma\alpha^2\right],\ g_{r2} = \frac{1}{b}\left(2\gamma\alpha + \alpha^2\right),\ g_{r3} = \frac{1}{b}\left(a - 2\alpha - \gamma\right) \tag{61a-c}$$

If γ is set equal to the decay rate of the actuator response a, then the modal gains for all the modes become

$$g_1 = -a\alpha^2/b,\ g_2 = (2a\alpha + \alpha^2)/b,\ g_3 = -2\alpha/b \tag{62a-c}$$

which are identical for all the modes. Introducing Eqs. (62) into Eq. (60), we obtain a linear feedback control law providing uniform decay rate for all the modes without altering the natural frequencies. Hence, modal estimation and implementation is bypassed entirely, although the formulation takes advantage of the concepts of modal control. In fact, uniform damping control can also be derived as a first-order approximation of natural control if

$$R = \frac{b^2}{2a^2\alpha^2} \tag{63}$$

and $\alpha << \omega_r$ for all modes.

As with other distributed control techniques, uniform damping control can only be implemented approximately with discrete actuators. However, this control method has the advantage of being applicable in a decentralized and collocated sense, and one that is known to be robust (Ref. 16). If an actuator and sensor pair is located at node i, acting

in direction ℓ, the control command force at that location takes the form

$$F_{ci\ell} = -m_{i\ell}(x_{i\ell}g_1 + \dot{x}_{i\ell}g_2 + \ddot{x}_{i\ell}g_3) \tag{64}$$

where $m_{i\ell}$ is an entry of the mass matrix, and $x_{i\ell}$, $\dot{x}_{i\ell}$ and $\ddot{x}_{i\ell}$ are correspondents of the displacement, velocity and acceleration vectors, respectively, all of which correspond to node i and direction ℓ. This is known as decentralized control because the force at a point is related only to measurements taken at that point and, of course, is only possible when the actuators and sensors are collocated. Comparing Eqs. (60) and (64), we conclude that the approximation involved in decentralized control consists of ignoring the off-diagonal terms in the mass matrix. If collocation is not possible, the measured state must be interpolated spatially to approximate the state at the actuator locations. Another advantage of uniform damping control is that all the modes are controlled, even with discrete actuation, not just a subset as with typical modal control techniques.

The mass matrix has been found to be the weighting matrix both for the open-loop maneuver forces, Eqs. (22), and for a particular closed-loop vibration control force, Eq. (60). There is a certain physical content in this result. Obviously, the uniform acceleration of a spacecraft demands more force at more massive sections. For the maneuver, this acceleration rate is the desired rotational acceleration and for the vibration control, it is the required vibrational decay rate α.

VII. NUMERICAL RESULTS

The SCOLE configuration of Fig. 2 was modeled by means of the finite element method. The nodal locations, each representing six

degrees of freedom, are denoted by the small circles. The mast supporting the antenna is a steel tube 10 feet long. The antenna consists of 12 aluminum tubes, each 2 feet long, welded together to form a hexagonal-shaped grid. The shuttle is simulated by a steel plate of uniform thickness with a mass of 13.85 slugs. The details of the model can be found in Ref. 2. The natural frequencies of the model in a space environment and cable detached are given in Table 1.

The maneuver strategy of Ref. 2 was applied to the rigid-body model of the spacecraft. The differential equation governing the actuator behavior was assumed to be of first-order, as in Eq. (27), with a = - 10 and b = 1. The histories of three rotational maneuvers about the x_0 axis are presented. The discrete-time switching history of a 0° to 30° minimum-time rotation with M_{max} = 20 lb-ft is illustrated in Fig. 3a. Note that the acceleration overshoots the target state because of the discrete-time switching. Figures 3b and 3c illustrate the continuous-time switching histories of 0° to 180° rotations with M_{max} = 20 lb-ft and M_{max} = 60 lb-ft, respectively.

To illustrate the effects of the actuator dynamics, the model is struck with an impulsive force of magnitude 5 lb in the y_0 direction. The structure is initially in a state of rest. The ensuing motion is modeled with 15 modes and the first 10 modes are controlled with natural control applied with distributed actuators and sensors. Both the classical form of natural control and natural control adapted to include the actuator dynamics is used to suppress the vibrations.

Figures 4a and 4b contain plots of the total energy of the system versus the control performance for various values of the actuator response decay rate a. The values of R in the performance functional

are 0.5 and 0.1 for Figs. 4a and 4b, respectively, while q = 1 in both cases, for all modes. The symbol + signifies a solution with classical natural control, in which actuator dynamics is not included. In all cases, the performance is improved with inclusion of actuator dynamics in the control formulation. Of course, as $a \to -\infty$ this difference approaches zero. Note that, comparing Figs. 4a and 4b, this difference also depends on the value of R. As R decreases, the modal decay rate increases according to Eq. (63). Hence, the benefits derived from including the actuator dynamics in the control formulation depend on the ratio of the desired modal decay rate to the actuators' decay rate. Of course, as this ratio is decreased, the effect of actuator dynamics becomes less important. As can be observed from a comparison of Figs. 3a-c, a similar conclusion can be made about the effect of actuator dynamics on the maneuver control. In this case, the ratio of interest is that of the mean angular maneuver velocity to the actuator decay rate.

The remainder of this section is concerned with the vibration control of the 30° and 180° roll maneuvers in space. The first fifteen modes are modeled for the simulations. Simulations are presented without vibration controls in Ref. 2, showing the excitation of the structure by centrifugal and tangential forces.

Figure 5 is a time-lapse plot of the spacecraft during the 30° roll maneuver without vibration control. The rotation is produced by actuators located on the shuttle, so that centrifugal and tangential forces cause structural vibration. The view is from directly behind the structure, showing the y_0z_0 plane with the x_0 axis directed into the paper. At each plotting sampling time, two plots appear, one in dashed

lines representing the structure as if it were rigid and the other representing the deformed structure. As the structure is accelerated, the appendage lags behind its desired position and then it bounces forward to precede the desired configuration during deceleration. When the maneuver ends, the appendage continues to vibrate about the desired target state.

The control techniques of Sec. 6 were applied to control the vibration of the spacecraft during the 30° roll. In all the presented cases, $R = 0.01$ and $q = 1.0$ for all the controlled modes. The time constant of the actuators' equations of motion was assumed to be $a = -10$, as in the maneuver strategy. Figure 6 is a time-lapse plot of the spacecraft during the maneuver with uniform damping control suppressing the vibrations of the first 9 modes using the ten actuators, six on the shuttle and four thrusters, two at the end of the mast and two at the antenna hub. Comparing Figs. 5 and 6, we conclude that uniform damping control during the maneuver provides excellent performance.

The spacecraft was maneuvered through the 30° angle with both distributed actuators and the 10 actuators discussed above. These 10 actuators were used for both maneuver control and vibration suppression. First, natural control approximated with projected actuating and distributed sensing was used. Next, 10 sensors were collocated with the actuators and the maneuver was repeated using natural control approximated by projected sensing and actuating. Finally, uniform damping control was used with the same 10 collocated actuators and sensors.

Figures 7a and 7b show the total energy in the system and the total command effort versus time, respectively, for all four of the above

mentioned control strategies. At the completion of the maneuver, energy is lower in all four strategies and the performance during the maneuver is always better compared to the case of no vibration suppression shown in Ref. 2. Distributed sensors and actuators yield the best performance by far. Note that uniform damping control performs almost as well as projected actuating and distributed sensing. This is to be expected, as the former is an approximation of the latter. However, it must be recalled that uniform damping control is decentralized and requires only a finite number of sensors, equal to the number of actuators.

The case of projected actuating and sensing is clearly inferior to uniform damping control, even though both techniques were applied with the same collocated sensors and actuators. The difference lies in the feedback method. Uniform damping control is decentralized, so that each sensor supplies information only for the collocated actuator, requiring no interpolation. On the other hand, the projected actuating and sensing strategy is centralized so that the modal states are estimated through interpolation of signals from all the sensors. The actuators are commanded from the estimated modal states. Hence, to reduce modal estimation error with projected sensing, more sensors are needed, as discussed in Sec. 6. Better modal filtering techniques can help to reduce the modal estimation error, but in general, more sensors than actuators are required.

The main control objective of the SCOLE project is aiming the antenna within a certain tolerance in minimum time. Hence, a study of the antenna rotations versus time is of interest. Figures 8a-c illustrate the instantaneous antenna rotations with respect to the frame $x_0y_0z_0$ about the x_0, y_0 and z_0 axes, respectively. The plots include

the responses produced during the maneuver with all four of the above control implementation techniques. The relative quality of performance is as mentioned above.

The effect of controlling only a finite set of modes is reflected in Fig. 8b in the form of residual motion of the uncontrolled modes. Uniform damping control dissipates energy in all of the modes, not just a finite set. From Fig. 8b, however, we observe that it is not very effective in controlling certain modes due to actuator placement. Nevertheless, with time, it does remove all of the energy from the system, unlike other implementation techniques.

In reality, because of saturation, actuators can only produce a finite amount of force or moment. The effect of limited command forces was investigated for the 30° roll maneuver and uniform damping control. The shuttle command forces and moments were limited to 2 lb and 20 ft-lb, respectively. The four thrusters on the appendage were each limited to 0.15 lb. These values correspond to saturation of the thruster on the antenna hub in the y_0 direction. Figure 10 contains plots of this command force versus time for limited and unlimited actuation. The corresponding plots of modal vibrational energy versus time in Fig. 11a show the adverse effect of command force truncation. The price for force truncation is increased vibrational energy as well as an associated increase in overall effort, as illustrated by Fig. 11b, although the control scheme is still effective.

The maneuver and control techniques are now demonstrated for a more extreme situation, a 180° roll maneuver with M_{max} = 60 ft-lb. From Fig. 3c, we conclude that this is a relatively severe maneuver in that a 180° roll, starting and ending at rest, takes place in less than 4 seconds.

Attempting this maneuver with actuators located only on the shuttle and without vibration controls resulted in deformations of the appendage exceeding greatly the small elastic motions assumption.

Natural control and uniform damping control were employed to suppress the vibration of the structure during the maneuver using R = .01 and q = 1.0. First, natural control was applied with distributed actuators and sensors to establish a "best case". Uniform damping control was then applied with the same 10 actuators and sensors used previously. Finally, uniform damping control was used with two additional thrusters (and collocated sensors), one in the z_0 direction at the hub of the antenna and the other at the extreme tip of the antenna in the y_0 direction.

The time-lapse plots of the structure during the maneuver showed no discernible deformations for all three control techniques. Figures 12a and 12b show the total modal energy and actual command effort versus time, respectively, for three control implementation techniques. Figure 12c illustrates the antenna rotation about the x_0 direction for all three cases. The addition of just two actuators resulted in much better performance and a reduction in effort of approximately 50%. Hence, the maneuver and vibration control approach is successful even in extreme situations and the necessary number of actuators depends on the performance requirements.

VIII. CONCLUSIONS

The perturbation method of solving the equations of motion permits the maneuver and vibration controls to be formulated independently. This eliminates the numerical difficulties encountered Refs. 3-5 when many modes are controlled. The quasi-modal equations of motion permit

an efficient vibration simulation as well as a straightforward vibration control formulation. Both uniform damping control and natural control were found to be effective in controlling vibration even during relatively quick maneuvers. The force distributions for both the maneuver control and uniform damping control depend exclusively on the mass matrix. Because the mass matrix is time invariant, these control formulations are not affected during the maneuver and, hence, are robust. The optimal actuator locations are the points of maximum mass both for maneuver and vibration controls. Actuator dynamics causes a time lag in force application, which degrades control performance. Including the actuator dynamics along with the structure dynamics in the control formulation minimizes this degradation.

REFERENCES

1. Meirovitch, L. and Quinn, R. D. "Equations of Motion for Maneuvering Flexible Spacecraft," Proceedings of the Fifth VPI&SU/AIAA Symposium on Dynamics and Control of Large Structures, Blacksburg, Virginia, June 12-14, 1985.

2. Quinn, R. D. and Meirovitch, L., "Maneuver Control and Vibration Simulation of Flexible Spacecraft," AIAA/ASME/ASCE/AHS 26th Structures, Structural Dynamics, and Materials Conference, San Antonio, Texas, May 19-21, 1986.

3. Turner, J. D. and Junkins, J. L., "Optimal Large-Angle Single-Axis Rotational Maneuvers of Flexible Spacecraft," Journal of Guidance and Control, Vol. 3, No. 6, 1980, pp. 578-585.

4. Turner, J. D. and Chun, H. M., "Optimal Distributed Control of a Flexible Spacecraft During a Large-Angle Maneuver," Journal of Guidance, Control, and Dynamics, Vol. 7, No. 3, 1984, pp. 257-264.

5. Breakwell, J. A., "Optimal Feedback Slewing of Flexible Spacecraft," Journal of Guidance and Control, Vol. 4, No. 5, 1981, pp. 472-479.

6. Baruh, H. and Silverberg, L., "Maneuver of Distributed Spacecraft," AIAA Guidance and Control Conference, Seattle, Washington, Aug. 20-22, 1984.

7. Hale, A. L. and Rahn, G. A., "Robust Control of Self-Adjoint Distributed-Parameter Structures," Journal of Guidance, Control, and Dynamics, Vol. 7, No. 3, 1984, pp. 265-273.
8. Meirovitch, L. and Baruh, H., "Control of Self-Adjoint Distributed-Parameter Systems," Journal of Guidance and Control, Vol. 5, No. 1, 1982, pp. 60-66.

9. Meirovitch, L. and Silverberg, L. M., "Globally Optimal Control of Self-Adjoint Distributed Systems," Optimal Control Applications and Methods, Vol. 4, 1983, pp. 365-386.

10. Meirovitch, L. and Baruh, H., "On the Robustness of the Independent Modal-Space Control Method," Journal of Guidance, Control, and Dynamics, Vol. 6, No. 1, 1983, pp. 20-25.

11. Meirovitch L. and Silverberg, L., "Control of Non-Self-Adjoint Distributed-Parameter Systems," Journal of Optimization Theory and Applications, Vol. 47, No. 1, 1985.

12. Meirovitch, L., Computational Methods in Structural Dynamics, Sijthoff & Noordhoff Co., The Netherlands, 1980.

13. Kirk, D. E., Optimal Control Theory, Prentice-Hall, Inc., Englewood Cliffs, NJ, 1970.

14. Meirovitch, L., Baruh, H. and Oz, H., "A Comparison of Control Techniques for Large Flexible Systems," Journal of Guidance, Control, and Dynamics, Vol. 6, No. 4, 1983, pg. 302.

15. Meirovitch, L. and Baruh, H., "On the Implementation of Modal Filters for Control of Structures," Journal of Guidance, Control, and Dynamics, Vol. 8, No. 6, 1985, pp. 707-716.

16. Silverberg, L., "Uniform Damping Control of Spacecraft," Proceedings of the Fifth VPI&SU/AIAA Symposium on Dynamics and Control of Large Structures, Blacksburg, Virginia, June 12-14, 1985.

Table 1 Natural Frequencies (Hz)

Mode	(Zero Gravity)
1	0.95626111
2	1.02205468
3	2.85798288
4	4.12238565
5	7.13573328
6	11.8067296
7	14.4703039
8	29.3765971
9	31.8650183
10	35.5681068

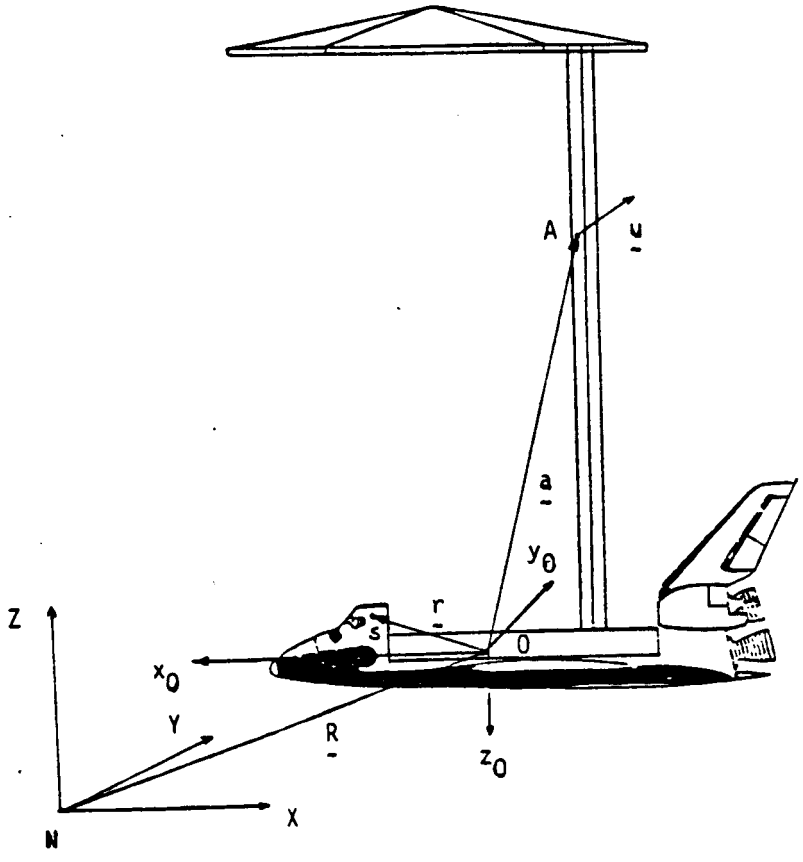

Figure 1. Spacecraft in Orbit

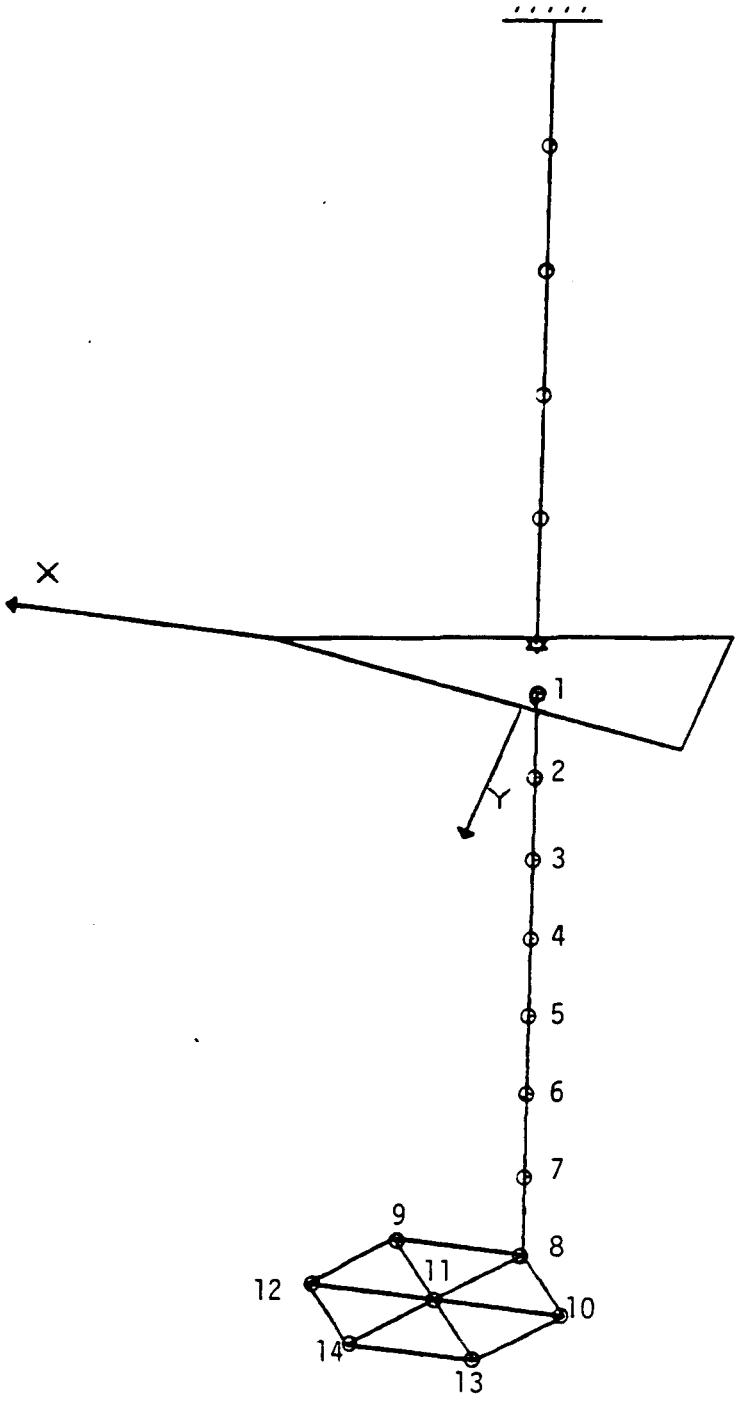

Figure 2. SCOLE Configuration Showing Nodal Locations

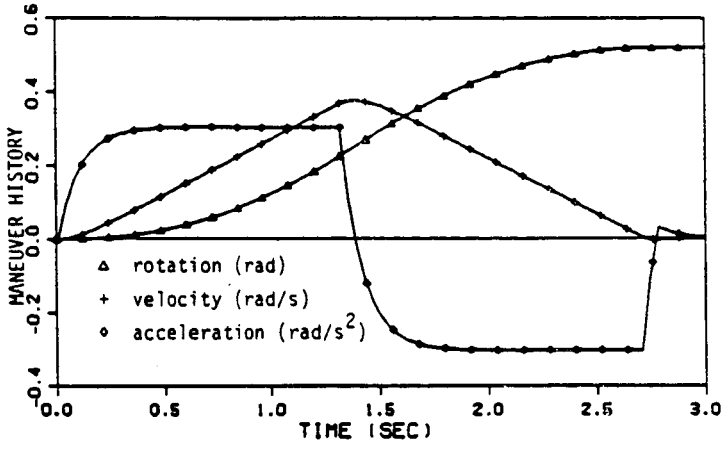

a) 30° roll, M_{max} = 20 ft-lb.

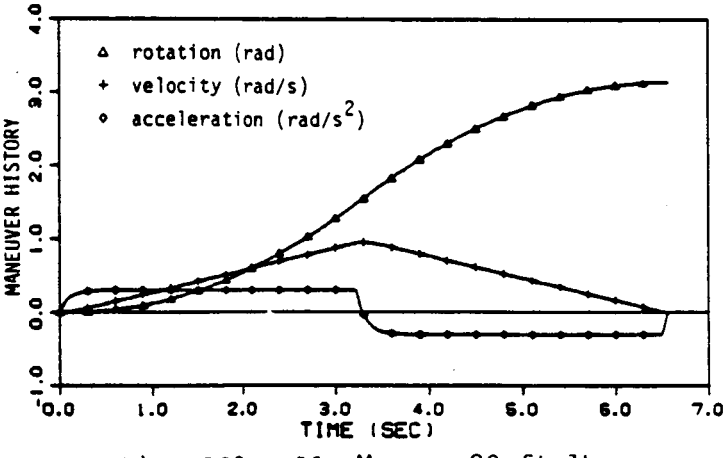

b) 180° roll, M_{max} = 20 ft-lb.

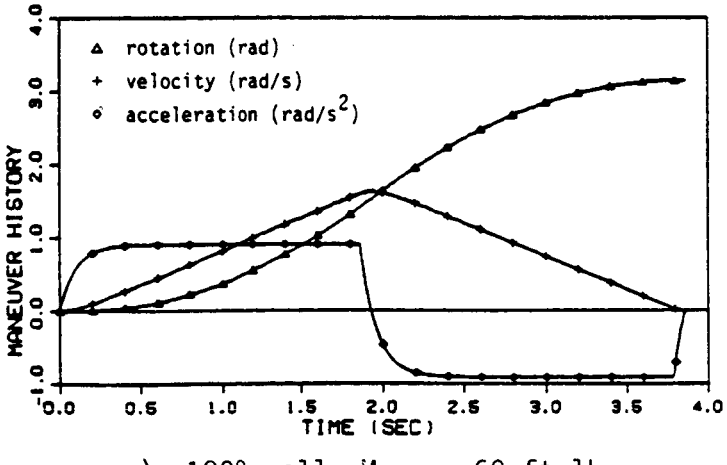

c) 180° roll, M_{max} = 60 ft-lb.

Figure 3. Comparison of Maneuver Strategies

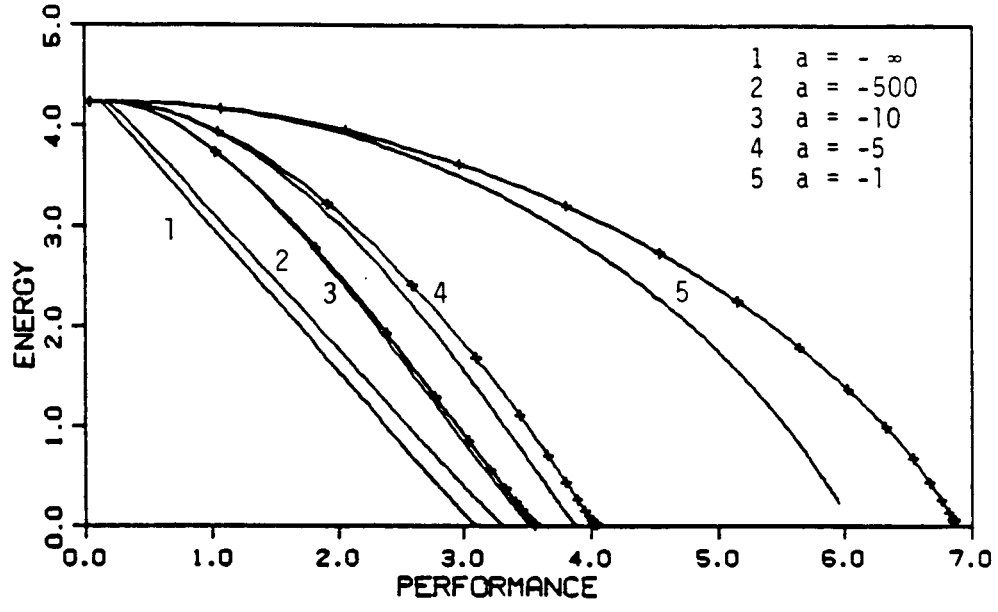

a) R = 0.5, g = 1.0.

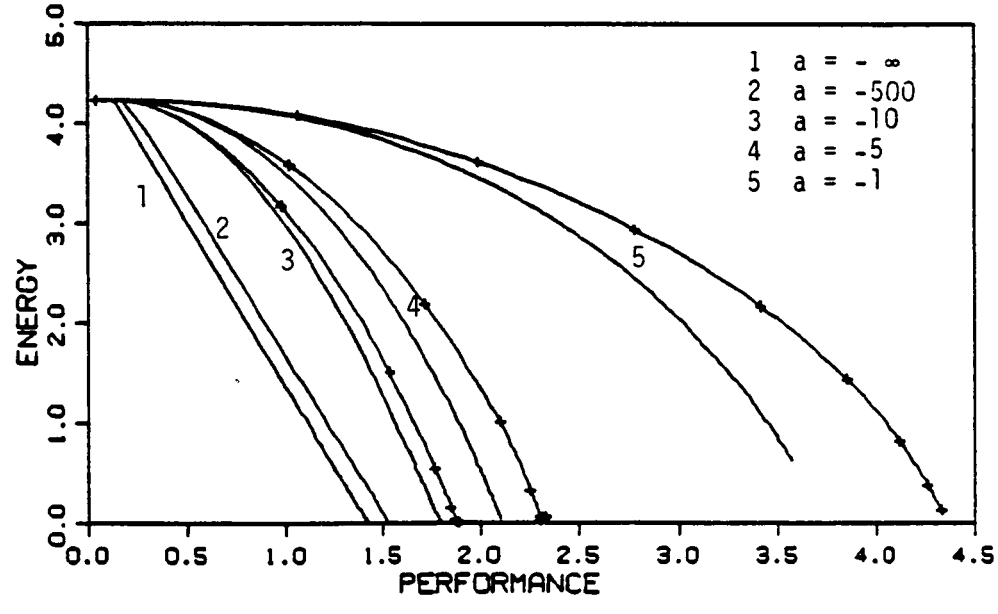

b) R = 0.1, g = 1.0.

Figure 4. Natural Control of an Impulse Response with Different Actuators

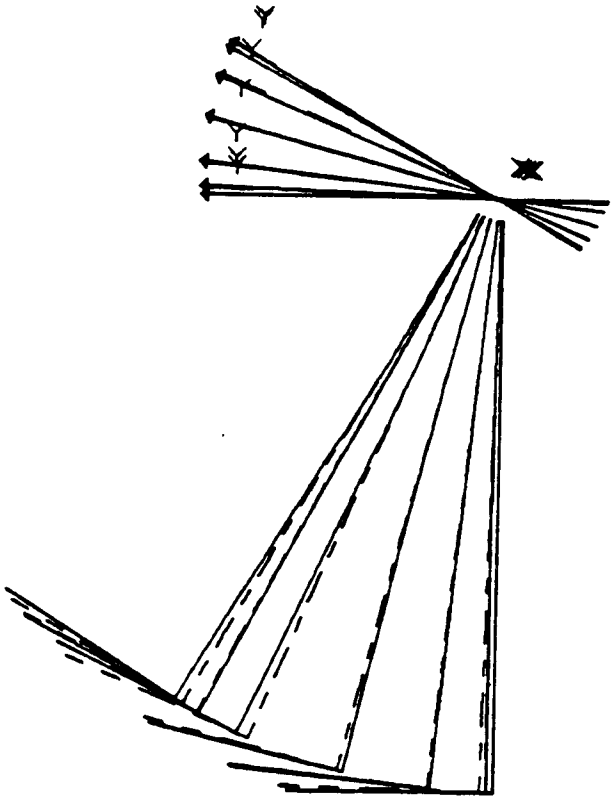

Figure 5. Time-Lapse Plot of 30° Roll Maneuver (No Vibration Control)

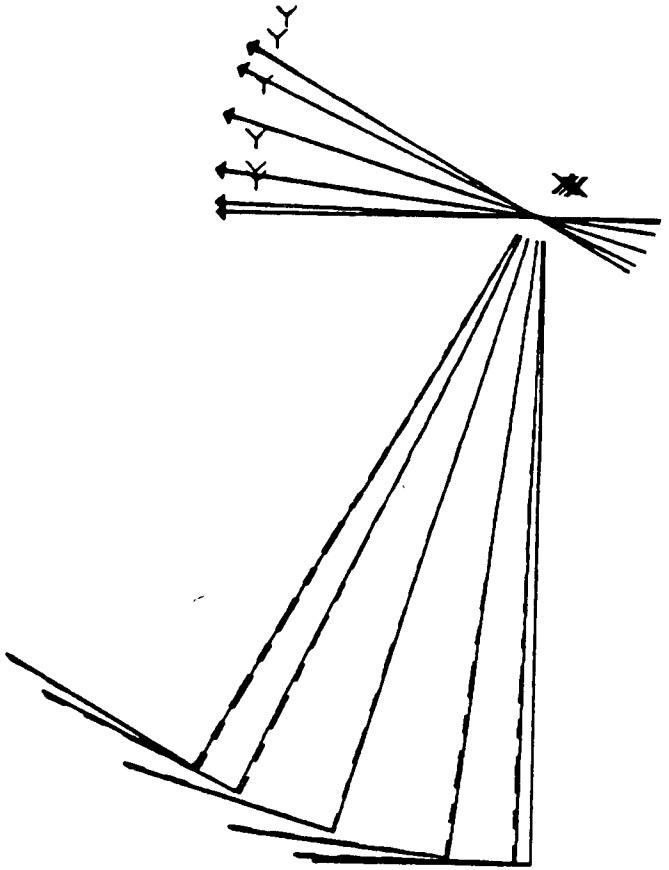

Figure 6. Time-Lapse Plot of 30° Roll Maneuver (Uniform Damping Using 10 Actuators)

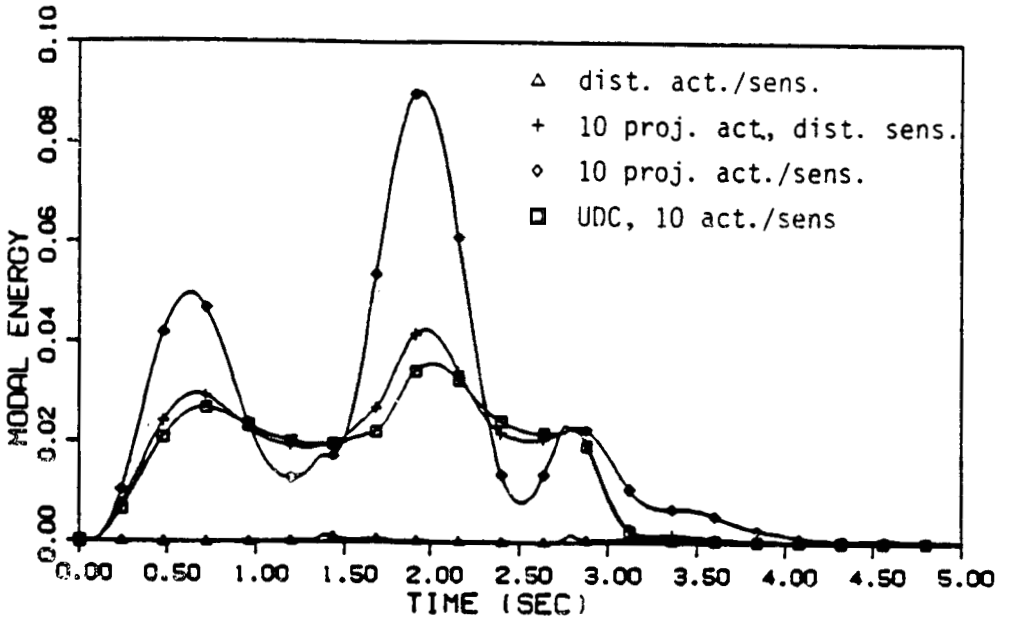

a) Energy

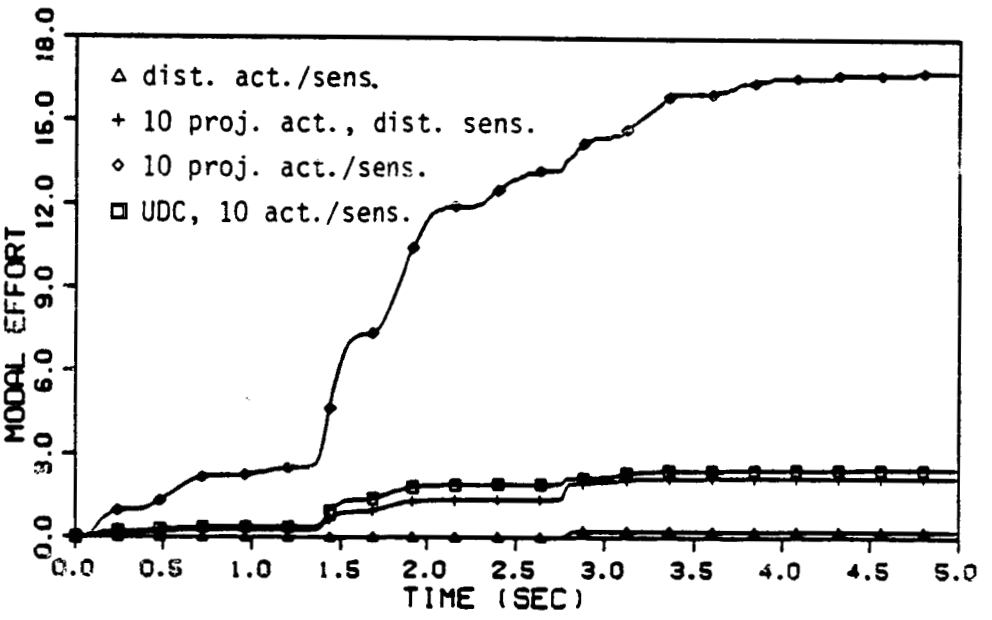

b) Effort

Figure 7. Comparison of Various Vibration Control Implementation Procedures for 30° Roll Maneuver

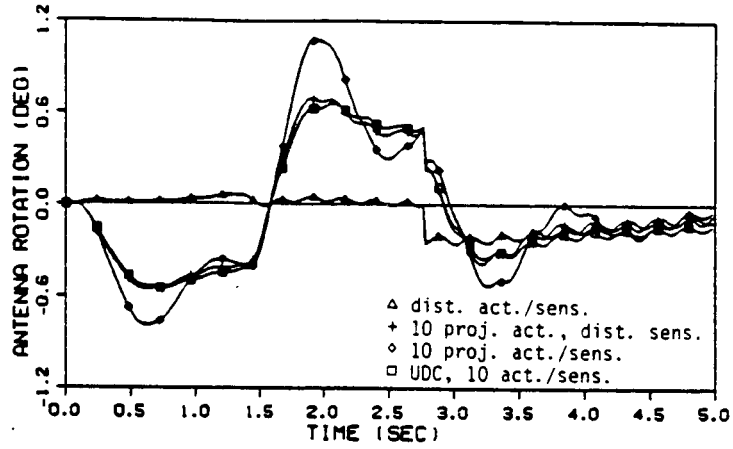

a) x_0 direction

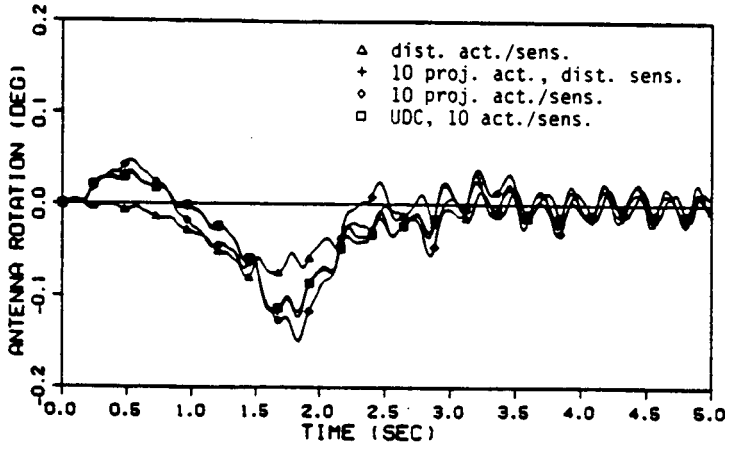

b) y_0 direction

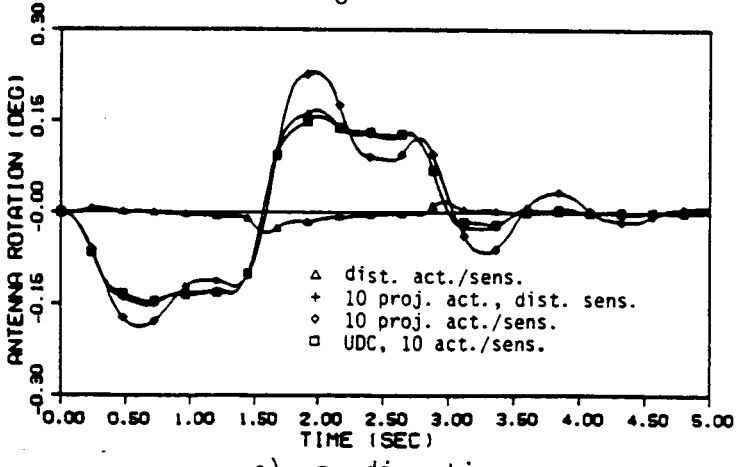

c) z_0 direction

Figure 8. Antenna Rotation During 30° Maneuver

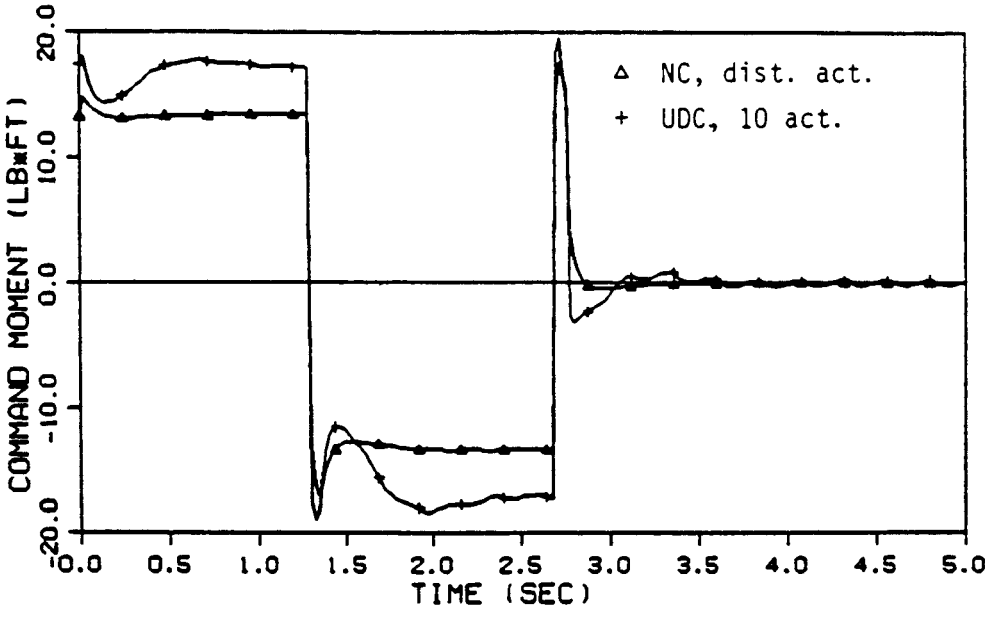

Figure 9. Torque on Shuttle in x_0 Direction During 30° Roll

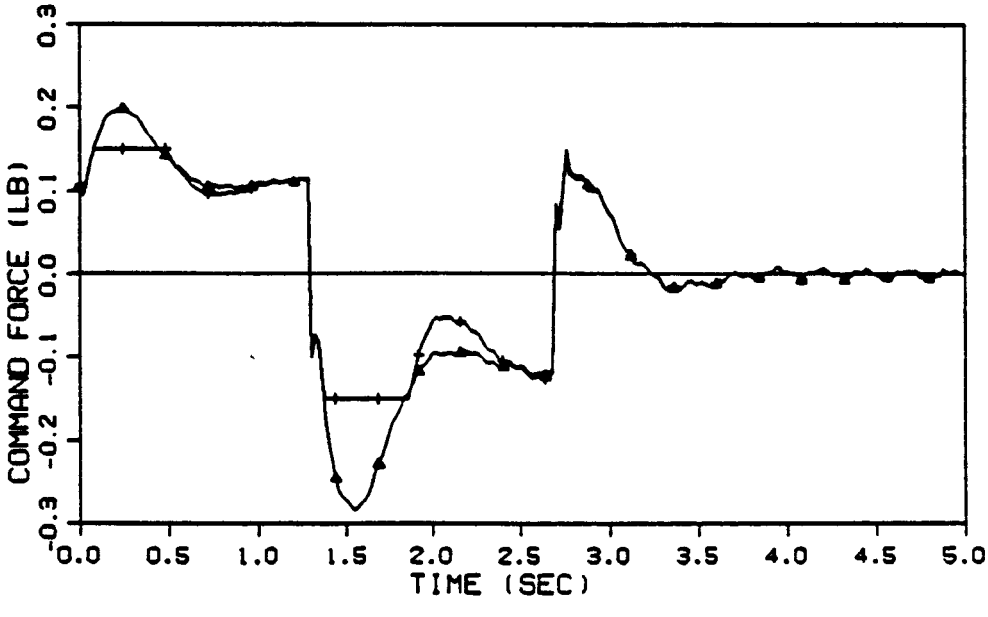

Figure 10. Force on Antenna in y_0 Direction with and without Thruster Saturation

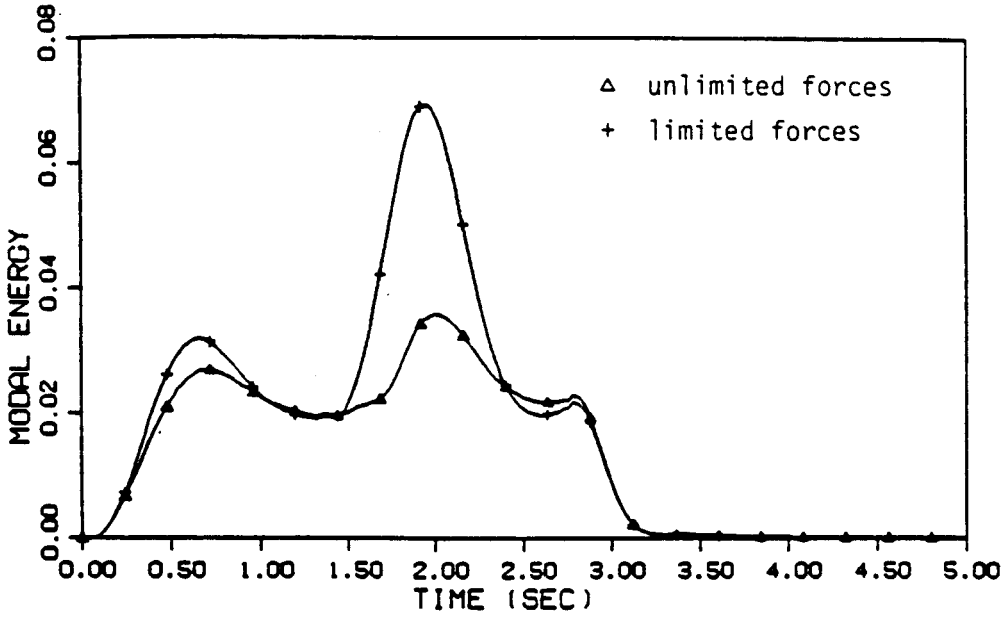

a) Energy

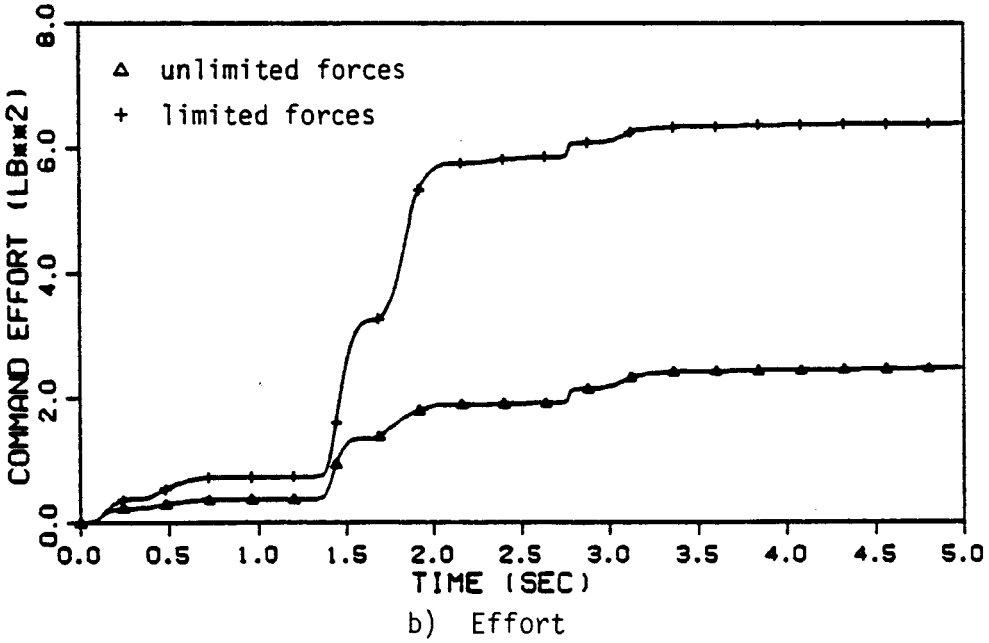

b) Effort

Figure 11. Effects of Actuator Saturation with Uniform Damping Control During 30° Maneuver

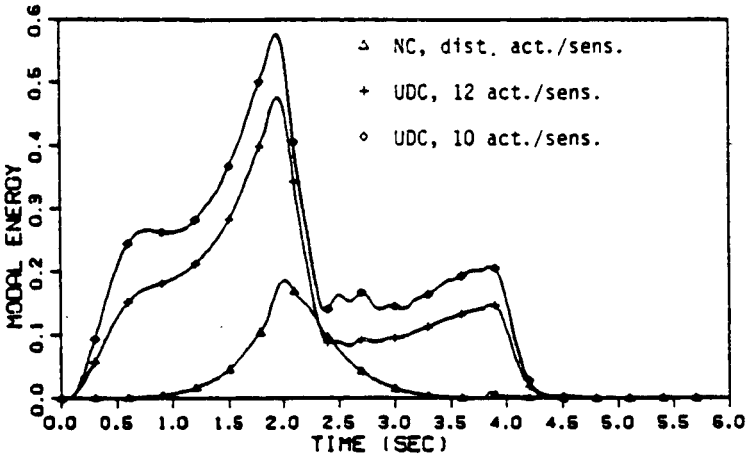

a) Energy

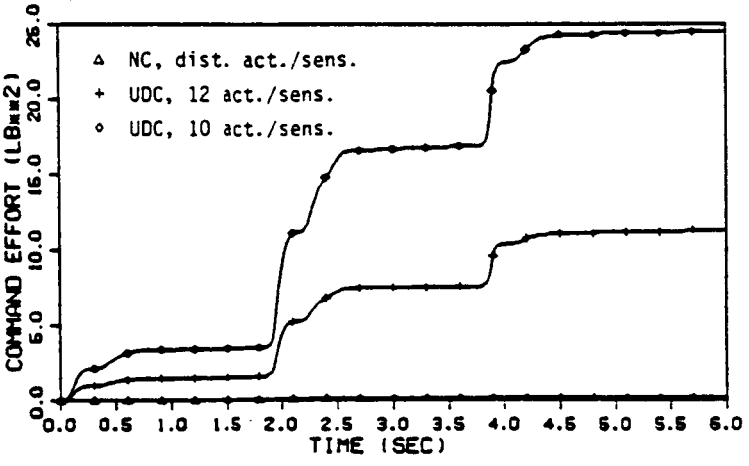

b) Effort

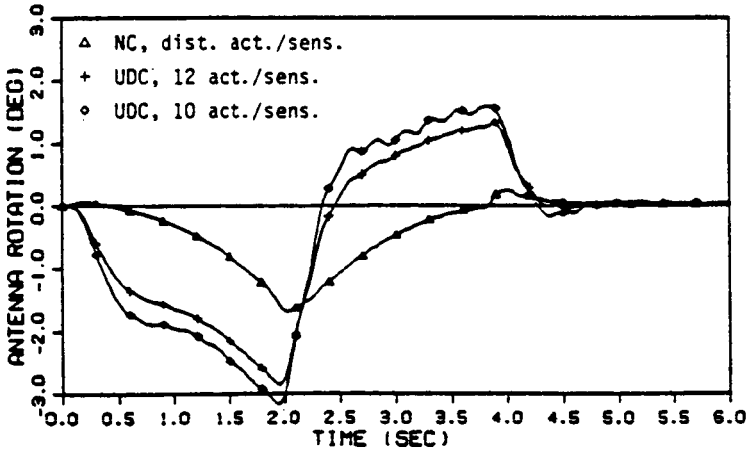

c) Antenna hub rotation in x_0 direction

Figure 12. Implementation of 180° Maneuver with Various Numbers of Actuators